Flow (2025), **5** E44
doi:10.1017/flo.2025.10037

FLOW CAMBRIDGE UNIVERSITY PRESS

RESEARCH ARTICLE

Understanding the effects of rotation on the wake of a wind turbine at high Reynolds number

Alexander Piqué[1], Mark A. Miller[1] and Marcus Hultmark[2]

[1]Pennsylvania State University, State College, PA, USA
[2]Princeton University, Princeton, NJ, USA
Corresponding author: Alexander Piqué; Email: axp5446@psu.edu

Received: 28 October 2024; **Revised:** 13 September 2025; **Accepted:** 17 November 2025

Keywords: wind turbine; high Reynolds number; hot-wire; tip vortex; wake meandering; wake recovery

Abstract

The wake of a horizontal-axis wind turbine was studied at a Reynolds number of $Re_D = 4 \times 10^6$ with the aim of revealing the effects of the tip speed ratio, λ, on the wake. Tip speed ratios of $4 < \lambda < 7$ were investigated and measurements were acquired up to 6.5 diameters downstream of the turbine. Through an investigation of the turbulent statistics, it is shown that the wake recovery was accelerated due to the higher turbulence levels associated with lower tip speed ratios. The energy spectra indicate that larger broadband turbulence levels at lower tip speed ratios contributes to a more rapidly recovering wake. Wake meandering and a coherent core structure were also studied, and it is shown that these flow features are tip speed ratio invariant, when considering their Strouhal numbers. This finding contradicts some previous studies regarding the core structure, indicating that the structure was formed by a bulk rotor geometric feature, rather than by the rotating blades. Finally, the core structure was shown to persist farther into the near wake with decreasing tip speed ratio. The structure's lifetime is hypothesised to be related to its strength relative to the turbulence in the core, which decreases with increasing tip speed ratio.

Impact statement

One constant trend with each new generation of wind turbines is their increasing size. We must improve our understanding of large-scale turbine wake interaction as the international community accelerates efforts to install turbines in closely packed wind farms. We discuss how the tip speed ratio affects a turbine's wake at high Reynolds numbers. First, lower tip speed ratios enhanced the tip vortex energy content and accelerated wake recovery. Second, the hub vortex was shown to be turbine rotation independent and rather a result of a bulk turbine geometric feature. Through a better understanding of how wind turbine operating conditions, like the tip speed ratio, affect a turbine's wake, designers can use these conditions in ways to improve wind farm power output. In the context of this manuscript, designers may consider operating wind turbines at tip speed ratios lower than their design conditions while balancing wake recovery and blade loading requirements.

1. Introduction

When wind turbines are organised as wind farms, it is common for some turbines to be in the wakes of others. A momentum deficit will be present in the inflow of those turbines as energy has been extracted by the upstream turbines, and consequently, the downstream turbine will be unable to extract as much energy from the wind as the upstream one. Therefore, the total power output and energy density of a wind farm depend on these turbine–turbine interactions.

Due to the complex geometry and large size of modern wind turbines, highly turbulent flow is expected in the wake, in combination with coherent flow structures generated by the rotor. This combination adds to our challenges in predicting and modelling these flows and systems. The flow structures play an important role in the wake recovery, which in turn limits the power density that can be achieved in a wind farm (Yang & Sotiropoulos, 2019*a*). At the tip of the blades, tip vortices are formed and shed into the wake in a helical fashion as they travel downstream, due to the blades' rotation (Porté-Agel et al., 2020). Flow structures confined to the core of the wake are also commonly present, and sometimes consist of discrete root vortices shed from the roots of the blades (Sherry et al., 2013*a*; Foti et al., 2016) or a hub vortex which is commonly characterised by a precessing helical vortex (Iungo et al., 2013; Kang et al., 2014). In addition, in some experiments a low-frequency behaviour has been observed in the wake, known as wake meandering. The mechanisms responsible for wake meandering are still being debated, but some theories include large-scale convection in the atmospheric boundary layer, (Larsen et al., 2007; Espana et al., 2011) or bluff-body-like shedding (Medici & Alfredsson, 2006; Okulov et al., 2014), with some authors postulating that both mechanisms are important (Heisel et al., 2018). The interactions between all three of these structures (tip vortex, wake meandering and coherent core feature) will dictate how the wake will recover its momentum (Okulov & Sørensen, 2007; Kang et al., 2014; Foti et al., 2016). Therefore, a strong understanding of how these structures are affected by different flow conditions, such as Reynolds number, tip speed ratio, turbulence intensity, etc. is imperative for more energy-efficient wind farms. There are two fundamental time scales governing the flow features in the wake: the turbine's angular velocity, ω, and the convective time scale D/U_∞, where D is a length scale associated with the geometry of the wake generator, here we will use the turbine diameter, and U_∞ is the free-stream velocity. A common non-dimensional parameter characterising the effect of the turbine's rotation rate is the tip speed ratio, $\lambda = \omega D\,(2U_\infty)^{-1}$. Tip speed ratio is one of the most important non-dimensional parameters governing wind turbine aerodynamics and the wake features. The tip speed ratio can be thought of as the ratio of the speed of the tip to the speed of the incoming flow, or as the ratio of the convective to rotational time scales.

In addition, λ has a strong effect on the turbine's performance metrics, such as the thrust, $C_T = T(0.5\rho A{U_\infty}^2)^{-1}$, and power, $C_P = P(0.5\rho A{U_\infty}^3)^{-1}$, coefficients. Here, T is the thrust force generated by the turbine, ρ is the fluid density, A is the area swept by the turbine and P is the power generated by the turbine. These performance metrics have a significant effect on the wake, as they characterise the power and momentum extraction from the flow. For example, C_T has been shown to have an effect on wake evolution (Whale et al., 2000) and shape (Eggleston & Stoddard, 1987). The power coefficient is also expected to influence the wake, but its influence is primarily due to its dependence on λ. The tip speed ratio sets the local angle of attack along the blade's span, and in turn, this affects the forces on the blades. The integral sum of the forces at each local airfoil section is responsible for the generation of power on a turbine. In turn, the local angle of attack of the airfoil section will set the vorticity shed into the wake, hence leading to a bulk wake effect.

Many previous studies have investigated the effects of λ on the wakes of wind turbines, but only a few of them have done so at Reynolds numbers, $Re_D = \rho U_\infty D\mu^{-1}$, relevant to modern wind turbines. Here, μ is the dynamic viscosity. As discussed above, local airfoil behaviour, such as lift, drag and stall, along a turbine's blade has an effect on the wake. Reynolds number has been shown to have an effect on an airfoil's lift curve, specifically in delaying stall for increasing Reynolds numbers (Devinant et al., 2002; Alam et al., 2010; Llorente et al., 2014; Pires et al., 2016; Brunner et al., 2021). In addition, it is well known that the Reynolds number affects transition (Tani, 1969; Narasimha, 1985), laminar separation bubbles (Gaster, 1967) and boundary layer statistics (Samie et al., 2018). Changes in separation bubbles and boundary layer behaviour will manifest as Reynolds number-dependent stall behaviour on a turbine's blade, leading to a Reynolds number-dependent near wake. Therefore, in order to properly understand the effects of λ on a turbine's wake, it is also important to maintain high Reynolds numbers. Although previous studies have found a lack of Reynolds number effects on the wake's mean velocity statistics (Chamorro et al., 2012; Piqué et al., 2022*b*), there is a scarcity of well-resolved measurements at high

https://doi.org/10.1017/flo.2025.10037 Published online by Cambridge University Press

Reynolds numbers and varying tip speed ratios. In the following section, the effects of rotation on the mean statistics, tip vortex, wake meandering and coherent core structures are summarised.

1.1. Effects of rotation

The wake statistics, specifically the mean velocity deficit and the variance, are significantly influenced by the tip speed ratio, due to its strong effect on C_T. In general, increasing C_T, increases the velocity deficit in the near wake, which has been observed in previous studies (Sherry et al., 2013*b*; Yang & Sotiropoulos, 2019*b*; El Fajri et al., 2022). In addition, it has been hypothesised that, with increasing λ, the turbine begins to increasingly resemble a solid disk, further explaining a larger deficit with increasing λ (Sherry et al., 2013*b*). However, other studies have observed a larger velocity deficit for smaller λ and C_T up to four diameters downstream (Bastankhah & Porté-Agel, 2016). An explanation for this contradiction is the smaller angle of attack experienced by the blades near the core at higher λ, which leads to a speed-up region in the core (Bastankhah & Porté-Agel, 2015). It is important to note that the detailed relationship between λ and C_T is unique to every turbine design. In addition to the mean velocity, the turbulence statistics are of utmost importance, both for the evolution of the wake itself, and due to the additional loads they generate on downstream turbines. As with the mean velocity deficit, the axial velocity variance is expected to have a dependence on C_T because of stronger velocity gradients associated with higher velocity deficits (Ceccotti et al., 2016).

The tip speed ratio has also been shown to affect the previously mentioned flow structures. The tip vortices have been shown to experience a more rapid collapse with increasing tip speed ratio (Troldborg et al., 2010; Sherry et al., 2013*a*; Lignarolo et al., 2014; Sørensen et al., 2015; Sarlak et al., 2016; El Fajri et al., 2022). The likely explanation for this behaviour is the decrease in the tip vortex pitch, or the distance between the successive vortex cores of the helical vortex system, with increasing λ (Wood, 1992; Ebert & Wood, 1999, 2001; Sherry et al., 2013*a*). Helical vortex instabilities were studied extensively by Widnall (1972). A critical finding relevant to wind turbines was that, with a small enough pitch, mutual inductance of the helical vortex is the most likely unstable mode. Therefore, this Biot–Savart driven mutual inductance would occur more closely to the turbine plane with decreasing pitch/increasing λ (Felli et al., 2011).

Furthermore, the influence of tip speed ratio on wake meandering has also been studied. Wake meandering is commonly identified as a convection dominated low-frequency event, that has been thought to require multiple diameters to develop. Thus, meandering is commonly characterised by a Strouhal number, $St = fDU_\infty{}^{-1}$, where f is the frequency of the meandering. Values range from 0.12 (Medici & Alfredsson, 2006) to values of the order of 0.3 (Chamorro et al., 2013; Howard et al., 2015). The Strouhal number has been shown to be independent of λ in the past (Yang & Sotiropoulos, 2019*b*), but a large enough λ is required to reach this invariant regime (Medici & Alfredsson, 2006).

Much like the effect on the tip vortices, the pitch of the root or hub vortices will decrease with increasing λ (Felli et al., 2011). Therefore, a more rapid collapse of the root vortex is also expected at higher λ, due to the same mechanisms responsible for the collapse of the tip vortex. Also, the root vortices have been found to become unstable before the tip vortices (Sherry et al., 2013*b*), which could be due to interactions with the nacelle boundary layer and consequent shear layer (Sherry et al., 2013*a*). Instead of discrete root vortices, numerous studies have identified a precessing helical hub vortex in the wake core (Iungo et al., 2013; Viola et al., 2014; Kang et al., 2014; Ashton et al., 2016). The precessing core feature has been shown to have a low-frequency time scale associated with it, but unlike wake meandering, there is still some debate over its dependence on the turbine's rotation rate. In Iungo et al. (2013), the ratio of the frequency of the hub vortex, f_{hub}, versus the turbine's angular velocity, f_{rot}, is relatively constant with tip speed ratio, and a numerical study that validated those findings found $f_{hub}/f_{rot} = 0.32$ (Viola et al., 2014). However, in another study, the time scale of the hub vortex was found to not have a direct relationship with the turbine's angular velocity, e.g. f_{hub}/f_{rot} is not a constant (Ashton et al., 2016). Therefore, questions still remain regarding the influence of the turbine's rotation on the hub vortex instability, a structure that is expected to be heavily dependent on the turbine's detailed geometry (Kang et al., 2014).

https://doi.org/10.1017/flo.2025.10037 Published online by Cambridge University Press

To summarise, a wind turbine's intrinsic rotation has an effect on its wake's bulk features, such as velocity deficit, and geometry-dependent flow structures, such as the tip vortex. Despite previous efforts to characterise the effects of rotation on a wind turbine's wake, there remains a lack of high Reynolds number studies on the topic. One objective of this investigation is to provide a tip speed ratio parametric study conducted at Reynolds numbers relevant to modern wind turbines. In this study, wake measurements of a model turbine are acquired for a range of downstream distances, $0.77 < x/D < 6.52$, and a range of tip speed ratios, $4 < \lambda < 7$. Throughout this manuscript, high λ will refer to conditions closer to $\lambda = 7$ and low λ will refer to conditions closer to $\lambda = 4$. The experiments were conducted at a constant Reynolds number, $Re_D = 4 \times 10^6$, which is at least an order of magnitude greater than previous wake experiments. Overall, these experiments produced a dataset that consists of the highest Reynolds number tip speed ratio parametric study of a wind turbine's wake. These datasets will serve as pertinent validation datasets for future numerical and computational simulations that seek to predict the wake of large-scale wind turbines. The results and discussion presented in this manuscript are based on the results and discussions presented in the author's thesis (Piqué, 2023).

2. Experimental set-up

The experimental investigation presented herein was conducted in the High Reynolds number Test Facility (HRTF) at Princeton University. Rather than solely using the flow speed to increase Reynolds number, which is the case in a conventional wind tunnel, the HRTF allows the static pressure, and thus fluid density, to be increased to obtain a desired Re_D. Pressures up to 238 bar and free-stream velocities up to 10 m s^{-1} are realisable in this flow facility. All tests were acquired at $Re_D = 4 \times 10^6$, but with different combinations of U_∞ and ρ. Dynamic similarity dictates that the non-dimensionalised statistical moments and spectra collapse as long as Re_D and λ remain constant, as has been shown previously by Piqué et al. (2022*a*,*b*). Upstream of the turbine, the flow is conditioned to produce a uniform inflow for the turbine. The free-stream turbulence intensity was 0.7 %. The turbine model had a diameter of 20 cm and consisted of NACA 63 series airfoils. A detailed description of the rotor blade geometry is provided in Miller et al. (2019). As the current study was performed using the same wind turbine and instrumentation set-up as used by Miller et al. (2019) and Piqué et al. (2022*a*,*b*), only a summary of the set-up is presented here. For a more detailed description see those references.

Thrust measurements were acquired using a JR3 Inc. six-axis load cell (model 75E20A4, 200N range) that was located at the bottom of the turbine tower, outside of the test section but inside the pressurised environment. All thrust data were acquired at 1000 Hz. An in-line torque transducer (Magtrol Inc., TM-305) was used to acquire both torque and angular velocity data. All data acquired from the torque transducer were sampled at 200 kHz. Due to the self-starting nature of the turbine, a magnetic hysteresis brake (Magtrol Inc. AHB-3) was used to control the rotational speed of the turbine. Free-stream velocity data were acquired using a Pitot-static tube that was located 0.74 m upstream of the turbine. Static pressure was measured using a pressure transducer (Omega Engineering Inc., PX419) and temperature was measured using a resistance temperature detector. The C_T and C_P curves can be found in figure 1 over the range of λ tested. Uncertainty in C_T never exceeded 6.8 %, C_P never exceeded 9.3 %, and λ never exceeded 2.7 %.

Axial velocity measurements in the wake were acquired using hot-wire anemometry. Due to the high Re_D and reduced physical size of the wake, compared with a field-scale turbine, conventional hot-wire anemometry would be insufficient for measuring the smallest turbulent length scales. To resolve a greater range of length scales in the turbine's wake, a nano-scale thermal anemometry probe (NSTAP) was used (Vallikivi & Smits, 2014; Fan et al., 2015). The NSTAP is fabricated at the Princeton Micro and Nano Fabrication Center (MNFC) using standard micro-electromechanical system techniques. The wire is composed of platinum and has dimensions of 60×2 μm $\times$ 100 nm. A silicon structure supports the free-standing wire. With the use of a commercial operating circuit (Dantec Dynamics A/S, Streamline), the NSTAP was operated in constant-temperature mode. Calibrations of the NSTAP were performed before and after every measurement of a velocity profile. Temperature changes never exceeded 0.4 °C over the

https://doi.org/10.1017/flo.2025.10037 Published online by Cambridge University Press

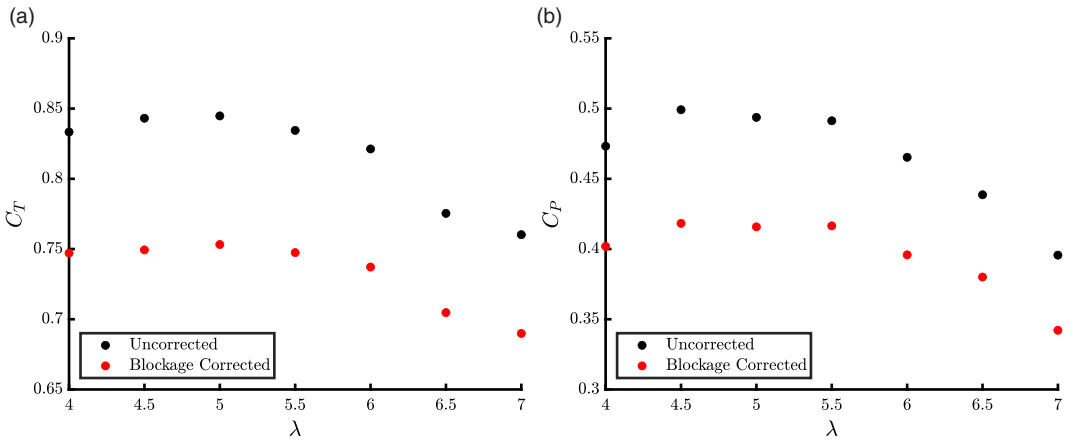

Figure 1. *The C_T (a) and C_P (b) curves of the studied turbine at $Re_D = 4 \times 10^6$. Uncorrected values are represented by black dots and blockage corrected values are represented by red dots. Blockage corrections were made following Bahaj et al. (2007). Due to the qualitative nature of the analysis, λ was not corrected for blockage.*

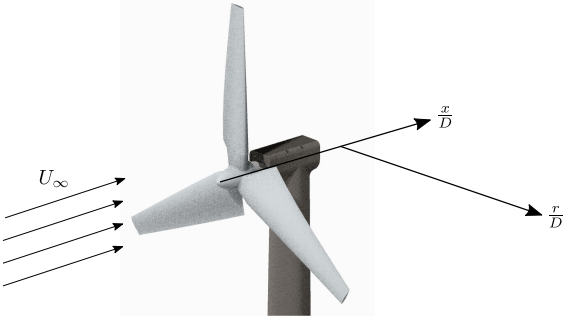

Figure 2. *Coordinate system of the presented wake results. Measurements were acquired along the r/D axis at different streamwise positions along the x/D axis. The turbine rotates clockwise.*

course of a wake measurement, so any temperature effects were deemed negligible. The repeatability in the hot-wire measurements was less than 0.15 %, estimated from the maximum difference between the pre- and post-calibration datasets. The NSTAP consisted of a single sensing element, so velocity measurements were limited to one-component measurements.

Wake measurements were conducted along the spanwise plane, $-0.86 < r/D < 0.86$, for at least 200 rotations of the turbine at each spanwise position. The coordinate system used in this study is presented in figure 2. Here, x/D denotes the axial direction, and r/D denotes the spanwise direction. A total of 81 points are sampled at $x/D = 0.77$ and 1.02 in order to improve the spanwise resolution of the tip vortex and 39 points were sampled at all other downstream positions. Mean axial velocity deficit and variance profiles are presented to aid a discussion of wake recovery and the effect of dominant flow structures on the wake's evolution. Spectral data are also analysed and presented to further the discussion on the effects of turbine geometry and rotation on the wake evolution.

3. Results

As discussed briefly in Section 1, C_T is expected to have an effect on the wake. As a result, it can be difficult to differentiate the sources of wake behaviour due to the tip speed ratio or the thrust coefficient

https://doi.org/10.1017/flo.2025.10037 Published online by Cambridge University Press

due to the intrinsic $\lambda - C_T$ relationship found for every turbine, as shown in figure 1(*a*). However, for the current turbine, the maximum change in C_T for $4 < \lambda < 6$ is no more than 2.9 %. Therefore, any trends observed in this range must primarily be an effect of the tip speed ratio, and thus the rotational effects. When considering the entire λ range tested ($4 < \lambda < 7$), the difference in C_T is no more than 11.1 %. Therefore, trends that appear only over this range of λ can be difficult to determine the root cause of. However, if a trend is observed for $4 < \lambda < 6$ and continues for $\lambda > 6$, the authors still consider this a tip speed ratio effect.

The results and discussion presented here are a natural extension to the previously conducted high Reynolds number parametric studies of the same model turbine as Piqué et al. (2022*a*,*b*). The tip speed ratio is one of the few operating conditions that can be toggled to control and predict turbine performance in a wind farm. Therefore, a tip speed ratio parametric study conducted at high Reynolds number is necessary to further improve wind farm operation and power output predictions. Some of the key findings of the previous studies were that the wake was populated by tip vortices that dominated the near wake ($x/D < 2.02$), wake meandering ($St = 0.3$) was identified at all downstream positions up to 5.5 diameters and a low-frequency wake core structure ($St = 0.6$) was observed only at the most upstream location $x/D = 0.77$. Furthermore, the tip vortex was shown to have a broadband effect on the turbulent energy content, which resulted in a reduced inertial subrange. The goal of the current study was to investigate how the wake is affected by varying tip speed ratio, at high Reynolds numbers, and whether it leads to changes in the evolution of the aforementioned wake structures or of the wake as a whole.

3.1. Characterising the wake

3.1.1. Wake recovery trends with tip speed ratio

Profiles of the mean deficit velocity are shown in figure 3 for the entire range of downstream locations and λ tested. To account for blockage effects, the deficit velocity is calculated as the difference between local velocity and the velocity outside of the wake at the tested downstream position, U_e. Due to hot-wire traverse limitations, it was difficult to acquire as many outside-wake measurements at 6.52 diameters downstream compared with 0.77 diameters downstream. Regardless, the general shape of the velocity profile shape was preserved and the most spanwise measurement was used to define U_e for 6.52 diameters downstream. First, there appears to be a change in the general shape of the deficit profiles in the range of $1.02 < x/D < 1.52$. To visualise this change, the profiles, when non-dimensionalised by conventional self-similar length scales, the half-width (l_0) and the deficit velocity ($u_0 = U_e - U(r = 0)$), as discussed by Townsend (1956), are shown in figure 4. The half-width is the spanwise distance between the centreline ($r/D = 0$) and the point at which the velocity deficit is $\frac{u_0}{2}$. It is clear that the wake transitions out of the very near wake somewhere in the range $1.02 < x/D < 1.52$, with a self-similar profile appearing beyond that. Figure 3 shows that the mean deficit velocity is independent of λ for $0.77 \leq x/D \leq 3.52$. However, for $x/D > 3.52$, the collapse starts to deteriorate with the $\lambda = 4$ and 5 cases showing a more rapid deviation, and the lowest λ case showing signs of a faster rate of wake recovery. The $\lambda = 6$ and 7 cases continue to collapse well with each other, but a greater downstream range may be needed to evaluate if this continues to hold further downstream.

The mean velocity deficit profile can be used to determine the thrust coefficient, given that the profile is acquired far enough downstream of the rotor, where the radial velocity and pressures can be assumed negligible. Given the consistent inflow conditions in the current study, the wakes of the studied turbine would be expected to collapse with enough downstream distance, due to the relatively small changes in C_T. However, for the presented turbine, the deficit profiles lose their self-similar behaviour for $x/D > 3.52$ and fail to obtain them by $x/D = 6.52$. Thus, the point at which one can calculate C_T from the deficit profiles, without additional information, is beyond the tested range.

3.1.2. Turbulence effects due to tip speed ratio

Profiles of the variance of the axial velocity are shown below in figure 5. At the most upstream locations, $x/D \leq 2.02$, the profiles exhibit four distinct peaks, whereas further downstream they exhibit only two

https://doi.org/10.1017/flo.2025.10037 Published online by Cambridge University Press

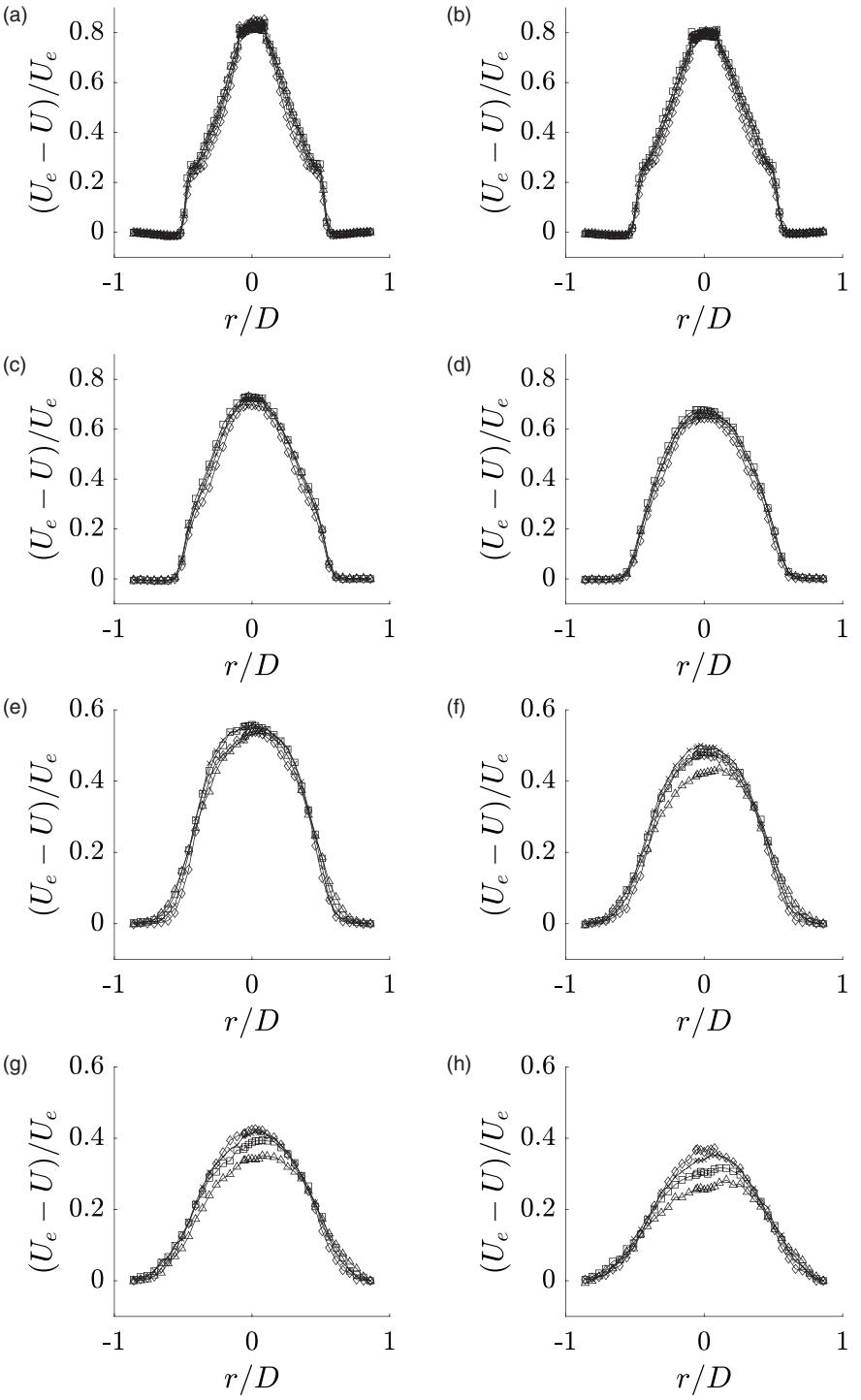

Figure 3. *Axial velocity deficit profiles across the tested downstream distances of x/D =0.77 (a), 1.02 (b), 1.52 (c), 2.02 (d), 3.52 (e), 4.52 (f), 5.52 (g), 6.52 (h) across all λ. Here, $\lambda = 4(\triangle)$, $\lambda = 5(\square)$, $\lambda = 6(\times)$, $\lambda = 7(\diamond)$.*

https://doi.org/10.1017/flo.2025.10037 Published online by Cambridge University Press

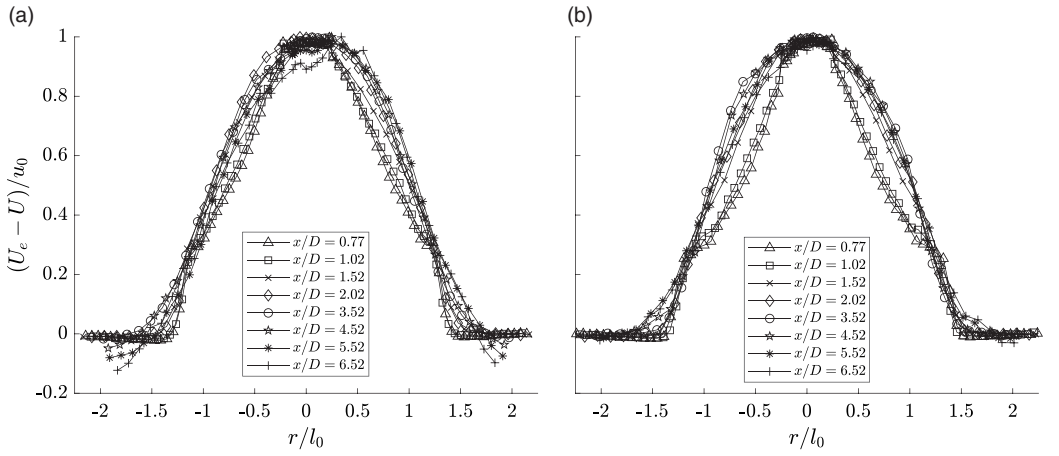

Figure 4. *Axial velocity deficit profiles across* $0.77 < x/D < 6.52$ *for* $\lambda = 4$ *in (a) and* $\lambda = 7$ *in (b). Profiles are non-dimensionalised by classical self-similar scales, the deficit velocity* (u_0) *and the half-width* (l_0).

peaks. The outer peaks, in the upstream locations, are indicators of the tip vortices and the inner peaks are signatures of an axisymmetric shear layer in the wake core. There is an asymmetry in the inner peak magnitudes, which is a still unexplained but a commonly observed phenomenon also in other wake studies (Odemark & Fransson, 2013; Schümann et al., 2013; Vinnes et al., 2022). Interestingly, for the two most upstream locations ($x/D = 0.77$ and 1.02), the entire profiles collapse with λ. Further downstream (starting at $x/D = 1.52$) the collapse starts to deteriorate and the higher λ cases see a decrease in the magnitude of the outer peaks (tip vortex signatures), whereas the inner region remains largely unchanged. The four-peak profile can still be observed up to $x/D = 2.02$, but with decreasing magnitude of the outer peaks corresponding to the decreasing strength of the tip vortices with increasing downstream distance (Hu et al., 2012). Increasing λ tightens the pitch of the helical vortex and reduces the strength of the tip vortices due to smaller angles of attack along the blade span. Both of these effects are expected to yield faster decay of the tip vortices with decreasing outer peaks, and lower variances in general, as a result.

When a tip vortex collapses, a burst of turbulent kinetic energy has been observed (El Fajri et al., 2022) and is thought to be due to increased entrainment from the 'leapfrogging' of the tip vortices (Lignarolo et al., 2015). At $x/D = 3.52$ (shown in figure 5*e*) the profiles have transitioned to a two-peak profile and have a greater magnitude than the peaks at $x/D = 2.02$, supporting previous findings of an increase in turbulent energy after the collapse of the tip vortex. The transition to a two-peak profile has been observed in past studies (Odemark & Fransson, 2013; Tedds et al., 2014; Sarlak et al., 2016), and indicates the point at which the near-wake structures have collapsed to form a single annular shear layer (Foti et al., 2016). The near wake is typically defined as the flow closest to the wake generator (turbine in this case) that is still dominated by turbine-dependent structures, such as tip and root vortices. The intermediate wake is a region where most of the near-wake structures have disappeared, but self-similar statistics are still not obtainable (Piqué et al., 2022*b*), and the far wake is where self-similarity is expected. As shown in Johansson & George (2006), the two-peak profile of an axisymmetric, non-rotating wake can persist into the far-wake region. Therefore, based on the variance profiles, the near wake can be expected to extend to at least $x/D = 2.02$ with the intermediate wake starting at a maximum of $x/D = 3.52$.

The failure of collapse that was first observed in the near-wake variance profiles, starting at $x/D = 1.52$, can also be observed in the intermediate wake, showing that the effect of λ and the breakdown of the tip vortex extends into the intermediate wake. In other words, initial conditions have an effect not only on the near wake, but also on the intermediate wake. For all downstream positions in the intermediate wake up to 5.52 diameters downstream, increasing λ correlates with a decrease in the magnitude of

https://doi.org/10.1017/flo.2025.10037 Published online by Cambridge University Press

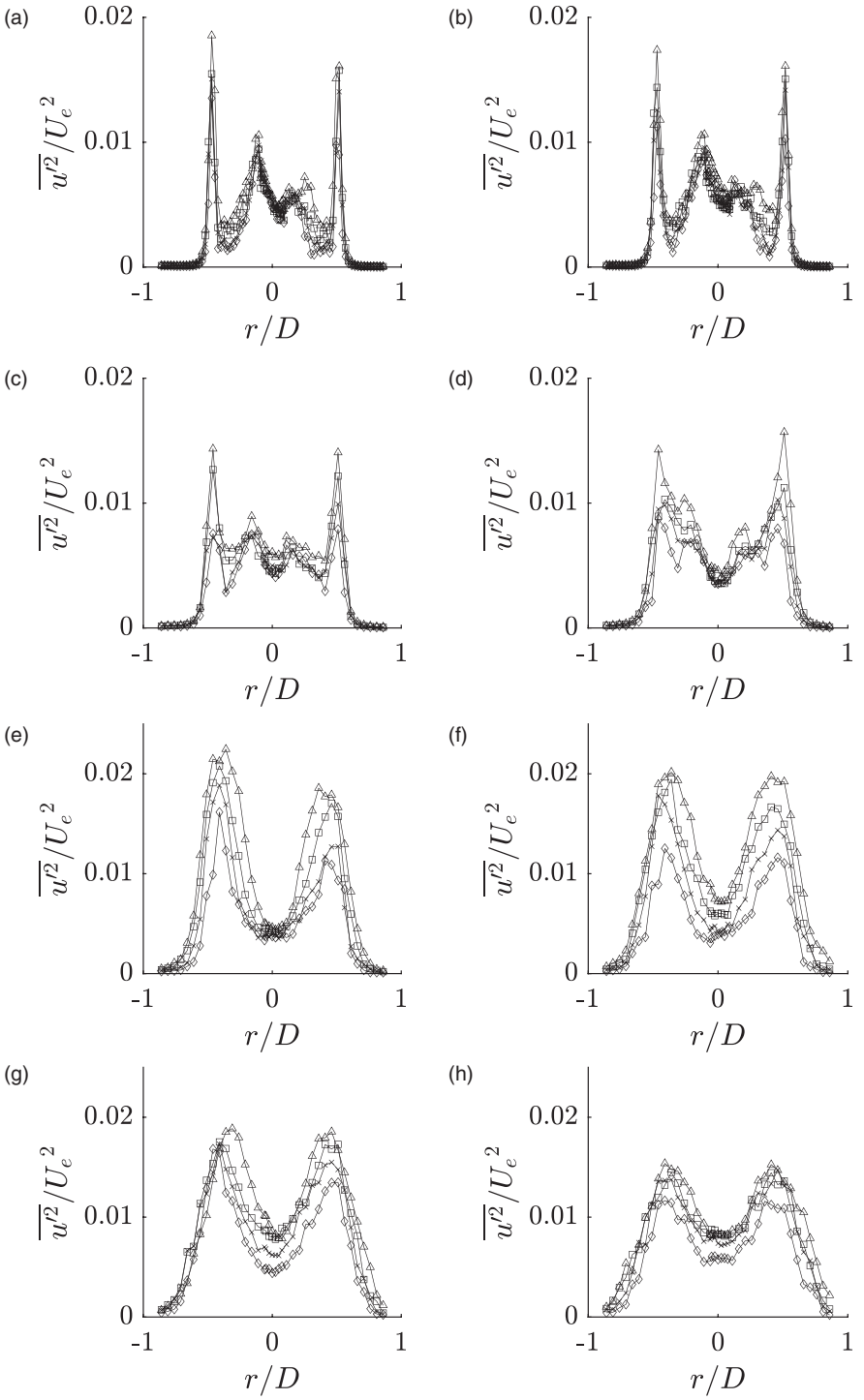

Figure 5. *Axial velocity variance profiles across the tested downstream distances of x/D =0.77 (a), 1.02 (b), 1.52 (c), 2.02 (d), 3.52 (e), 4.52 (f), 5.52 (g), 6.52 (h) across all λ. Here, $\lambda = 4(\triangle)$, $\lambda = 5(\square)$, $\lambda = 6(\times)$, $\lambda = 7(\diamond)$.*

https://doi.org/10.1017/flo.2025.10037 Published online by Cambridge University Press

the two dominant peaks. As shown in figure 5, the greater the tip speed ratio, the smaller the variance, with the most notable trend for $1.52 < x/D < 5.52$. The initial burst of turbulent kinetic energy after the collapse of the tip vortex will decay due to recovery mechanisms, such as entrainment from surrounding regions. Therefore, it is likely that the higher turbulence levels in the vicinity of the tip vortices, will accelerate wake recovery for lower λ, as shown in figure 3. Based solely on the variance profiles, it is difficult to determine whether the tip vortex alone is responsible for the λ dependence observed. However, the dependence on λ decreases further downstream, until the point at $x/D = 6.52$, where the variance profiles have almost collapsed once again.

As discussed in Section 3, C_T remains relatively unchanged over the range of tested λ. For any one C_T value, there is not a single unique force distribution along the blade. The force distribution along a rotor's blade is dependent on the angle of attack of the local airfoil section, which in turn depends on the turbine's tip speed ratio. In addition, the local angle of attack will determine the vorticity shed into the wake, thus affecting the strength and distribution of vortical structures being shed into the wake. Therefore, it is expected that the turbine's rotation will affect both the local vorticity and the dominant wake flow structures (such as tip or hub vortices). For the studied turbine, vortical structures formed in the near wake show significant rotational effects throughout the tested regime, specifically the turbulence levels in the near and intermediate wake associated with the tip vortex, as shown in figure 5. These effects cannot be attributed to C_T, as it is almost constant. A thorough investigation of the energy spectra will provide more clues as to the λ relationship and its effects on wake evolution.

3.2. Periodic structures

As discussed in Section 3.1.2, the turbulence generated by the tip vortices at the wake's edge is hypothesised to be an important mechanism for wake recovery. However, it is difficult to determine the effects of other dominant flow structures, such as wake meandering and coherent core phenomena, on the wake recovery and their relationship with the tip speed ratio. Therefore, a spectral analysis of the flow near the wake's edge and core was conducted to determine how λ affects the tip vortex and core structures, respectively. Here, the spectra are non-dimensionalised by f_{rot} or by the convection time scale (yielding a Strouhal number, St). The different non-dimensionalisations are used to determine if a periodic structure is governed by the rotation of the blades or by flow convection.

3.2.1. Tip vortex

In figure 6, spectra near the tip vortex location ($r/D = 0.519$ and $x/D = 0.77$) are shown. In figure 6*a* the frequencies are non-dimensionalised as a Strouhal number, with a peak present at $St \approx 0.3$, which corresponds to the wake meandering reported in previous studies. The St value of that peak remains close to constant across all λ, which agrees with the earlier observations of wake meandering (Medici & Alfredsson, 2006; Yang & Sotiropoulos, 2019*b*). Also, the magnitude of the wake meandering peak decreases with increasing λ. In figure 6(*b*), the frequencies are instead non-dimensionalised by f_{rot}. Here, the influence of the tip vortex can be more clearly observed. Strong peaks are identified at multiples of f_{rot} (f_{rot}, $2f_{rot}$ and $3f_{rot}$). It can also be seen that the tip vortices have a strong broadband effect for frequencies greater than f_{rot}. This range is similar across all λ tested for $x/D = 0.77$. The turbine's tip vortices push the inertial subrange to higher reduced frequencies, with an increased broadband energy content. Therefore, the broadband energy strengthening effect of the tip vortex further supports the previous hypothesis that the tip vortex has a lasting effect on wake recovery.

From Section 3.1.2, the magnitude of the tip vortex signature in the variance was found to decrease with increasing λ. Since there was a monotonic trend with λ, only the spectra at $\lambda = 4$ and 7 are shown in figure 7 to more clearly illustrate the trends with tip speed ratio. When considering the near wake, it is clear that the tip speed ratio's influence over all reduced frequencies is much stronger at $x/D = 2.02$ than at $x/D = 0.77$. As shown in figure 7, the overall energy content near the blade tip decreases with increasing tip speed ratio. This trend of decreasing energy with increasing λ corresponds to the lower

https://doi.org/10.1017/flo.2025.10037 Published online by Cambridge University Press

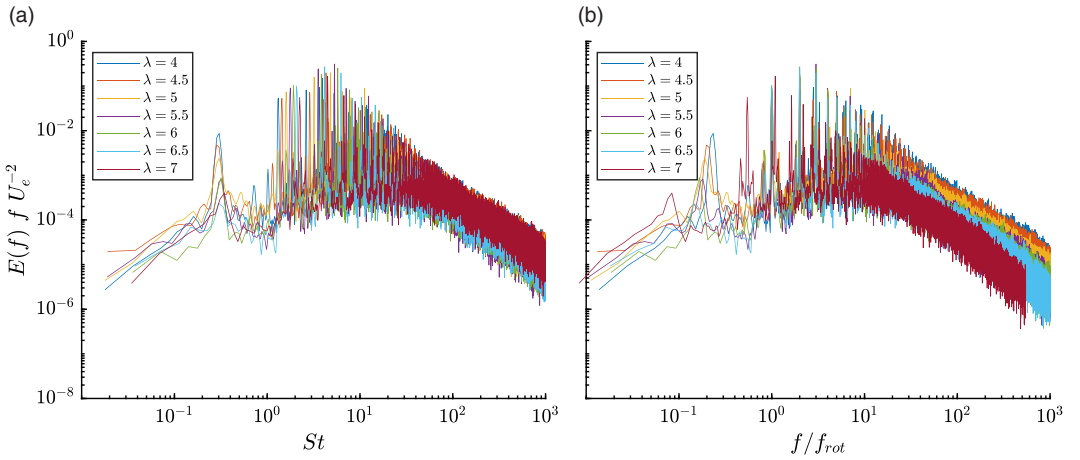

Figure 6. *Premultiplied spectrum at $x/D = 0.77$ and $r/D = 0.519$, a location near the tip vortex. The frequency is non-dimensionalised by a Strouhal number (a) or by the rotational frequency of the turbine, f_{rot} (b).*

variance magnitudes observed in Section 3.1.2. At the most upstream location, $x/D = 0.77$, there is only a weak λ dependence (and possibly none at the lower reduced frequencies), agreeing well with the collapse of the axial variance profiles for the same downstream position. The broadband effect of the tip vortices alters the turbulence and shifts the inertial subrange (as identified by the dashed lines in figure 7) to smaller length scales, but the affected frequency range decreases with increasing downstream distance, within the near wake.

Premultiplied spectra at $x/D = 3.52$ and $x/D = 6.52$ are shown in figures 7(c) and 7(d), respectively. The lower λ case shows a greater energy content across all scales at $x/D = 3.52$, supporting the hypothesis that the turbulence generated by the tip vortices in the near wake also affects the intermediate wake. This trend was discussed in Section 3.1.2 and is found in the greater magnitude variance profiles for smaller λ of figure 5(e). At $x/D = 6.52$, shown in figure 7(d), the trend with λ is less pronounced, especially for $f/f_{rot} < 3$, the region most affected by the tip vortex, representing a large fraction of the total energy (recall the collapse of the variance profiles at the $x/D = 6.52$ in figure 5h).

3.2.2. Persistence of coherent wake core structures

In figure 8, the premultiplied spectra in the wake core, $r/D = 0.007$ and $x/D = 0.77$, are shown for different λ. Two clear peaks can be observed, one at $St = 0.3$ and one at $St = 0.6$. Wake meandering is typically associated with $St = 0.3$ and, as mentioned in Section 3, the $St = 0.6$ peak is a signature of shedding in the wake core. As discussed in Section 1, wake core structures have been identified and are hypothesised to be signatures of the root vortex or a precessing helical vortex. From figure 8(b), there is no collapse associated with any of the harmonics of f_{rot}, and therefore it is unlikely that there are any root vortices at $x/D = 0.77$ for any tip speed ratios tested. A precessing helical vortex in the wake core has been identified in previous studies, which showed that there is a dependence on f_{rot} (Iungo et al., 2013). However, for the case of the presented turbine, no such structure is observed. The $St = 0.6$ signature remains constant for all λ tested, suggesting that a bulk feature of the turbine, rather than blade-driven formation mechanisms, is driving the wake core structure observed at $St = 0.6$.

As discussed in Piqué et al. (2022a), the structure at $St = 0.6$ is short lived, and only present in the very near wake of the turbine. Figure 9 shows the premultiplied spectra at $x/D = 1.02$ and $x/D = 1.52$. Once again, the wake meandering and wake core structures have a constant St with changing λ. However, it is clear that with increasing λ the magnitude of the $St = 0.6$ event decreases, until the point where the signature disappears. In figure 9(b), at $x/D = 1.52$, the $St = 0.6$ signature is only evident at the

https://doi.org/10.1017/flo.2025.10037 Published online by Cambridge University Press

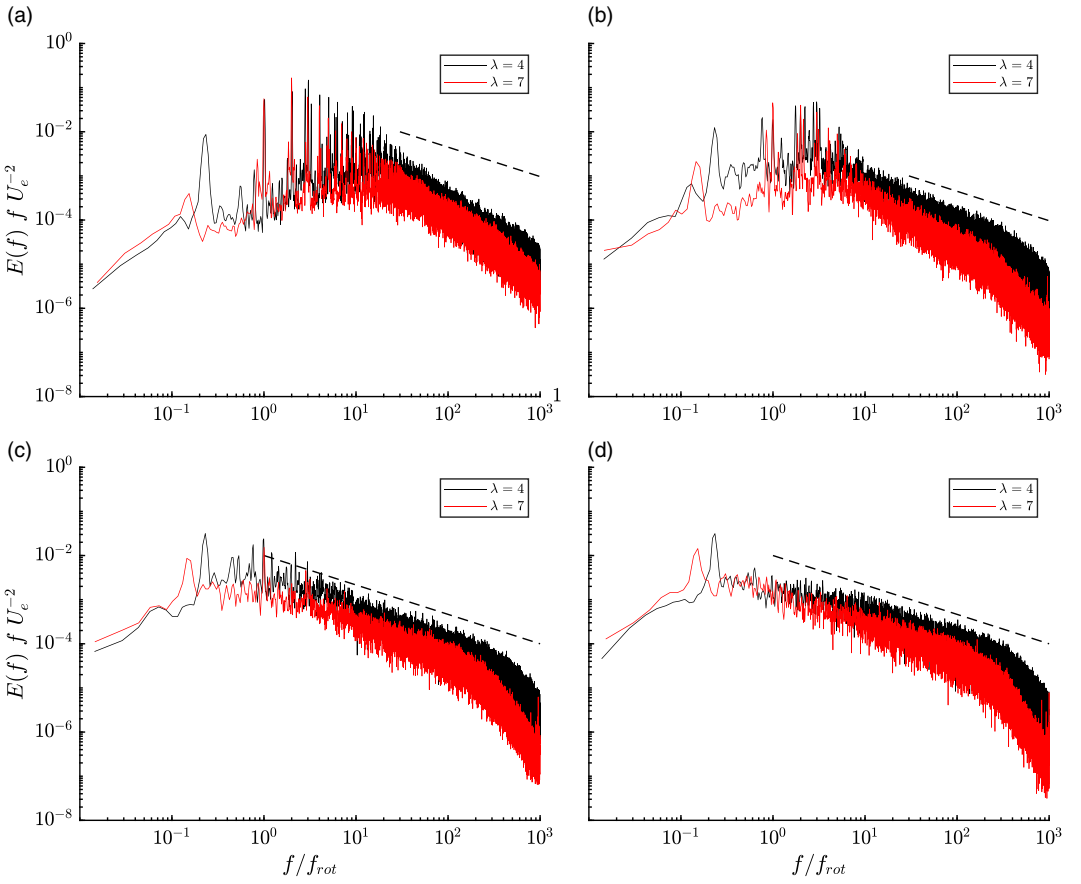

Figure 7. *Premultiplied spectra at (a) $x/D = 0.77$, (b) 2.02, (c) 3.52 and (d) 6.52 . The spectra are obtained near the location of the tip vortex, but due to the different spanwise resolutions for the downstream positions, the radial position is slightly different. In (a), $r/D = 0.519$ and in (b–d), $r/D = 0.51$. Dashed lines represent a −2/3 slope, a reference to the inertial subrange in premultiplied spectrum scaling.*

lowest λ. For all further downstream locations, the signature of the $St = 0.6$ event has disappeared. Therefore, the lifetime of the core structure is dependent on the tip speed ratio, where a lower λ prolongs the downstream extent of the structure. Also, unlike the tip vortex, the tip speed ratio does not have a strong effect on the energy content of any of the other scales in the core. This observation was expected due to the strong degree of collapse of the variance profiles in the wake core in the near wake, as discussed in Section 3.1.2.

3.2.3. Spanwise extent of the wake core signature

In this study, the $St = 0.6$ signature has been shown to be affected by the tip speed ratio, such that it has a smaller downstream extent and is weaker with increasing λ. To further visualise the trend between λ and the strength of the low-frequency features (wake meandering and the core structure), the premultiplied spectra presented as a contour plot are shown in figure 10. A principal feature of the spectrum is that increasing tip speed ratio leads to a reduction in the strength and spanwise influence of the wake meandering and core structure features. To better visualise the trend between λ and the core structure's strength, the peaks in the premultiplied spectrum in the Strouhal number range of $0.55 < St < 0.65$, Φ_c, have been identified in figure 11. In figure 11(a) the premultiplied spectrum is non-dimensionalised

https://doi.org/10.1017/flo.2025.10037 Published online by Cambridge University Press

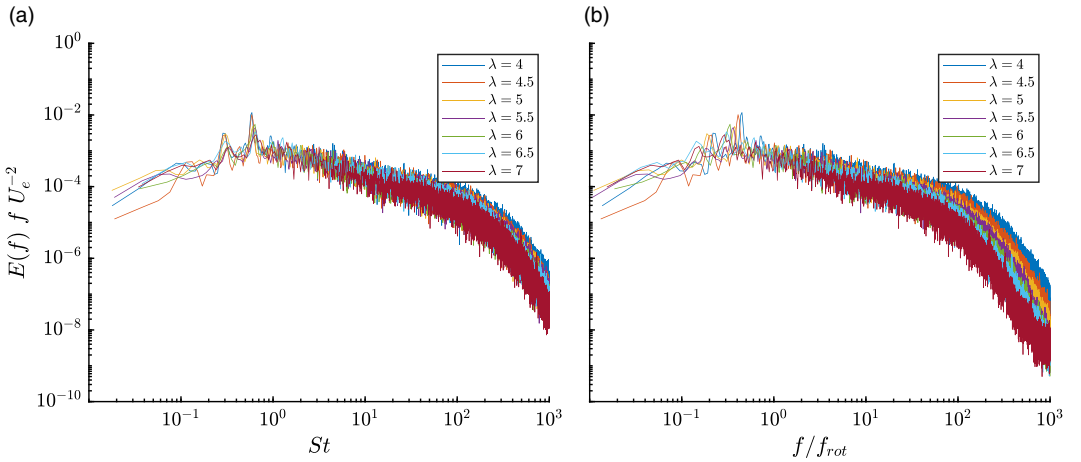

Figure 8. *Premultiplied spectrum at $x/D = 0.77$ and $r/D = 0.007$, a location in the wake core. The frequency is non-dimensionalised by a Strouhal number (a) or by the rotational frequency of the turbine, f_{rot} (b).*

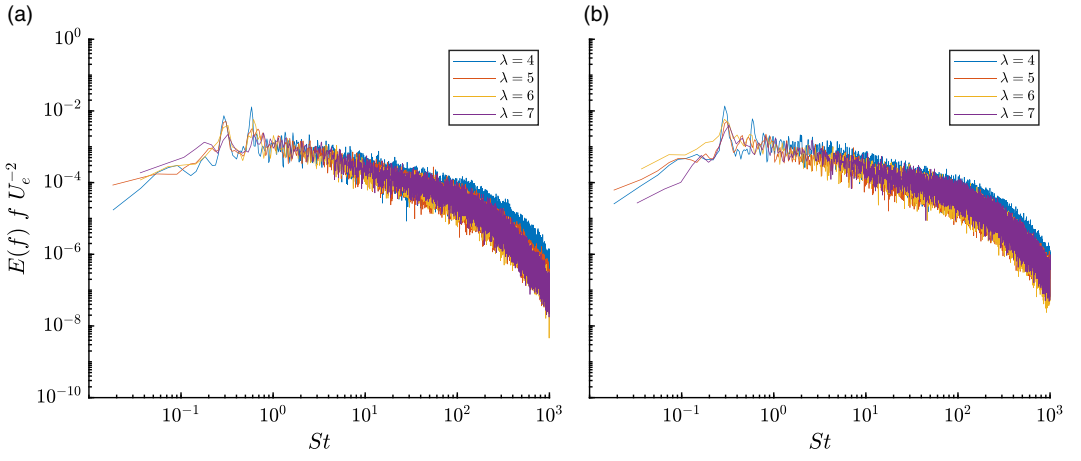

Figure 9. *Premultiplied spectrum at (a) $x/D = 1.02$ and $r/D = 0.007$ and (b) $x/D = 1.52$ and $r/D = 0.01$. There is a slight mismatch in the spanwise position due to a different spanwise resolution between the two downstream locations.*

by the maximum value of the spectrum, $\Phi_{c,max}$, to better visualise the spanwise extent of the wake core signature. In figure 11(*b*) the premultiplied spectrum is non-dimensionalised by the variance at the centreline, $u_c'^2$, to better visualise the strength of the core structure relative to turbulence in the core. From figure 11(*a*), the wake core signature is found to have a similar radial extent, independent of λ. Despite the tip speed ratio invariance of the spanwise length scale of the wake core signature, the tip speed ratio has a strong effect on the strength of this structure. In figure 11(*b*) the strength of the wake core structure is shown to decrease with increasing tip speed ratio, and can be expected to have a smaller effect on the flow in the core. This trend helps support the previous finding from Section 3.2.2 that the downstream lifetime of the wake core signature decreases with increasing λ; for the studied turbine, the strength of the wake core signature relative to the turbulence in the core decreases with increasing λ, leading to a faster collapse.

https://doi.org/10.1017/flo.2025.10037 Published online by Cambridge University Press

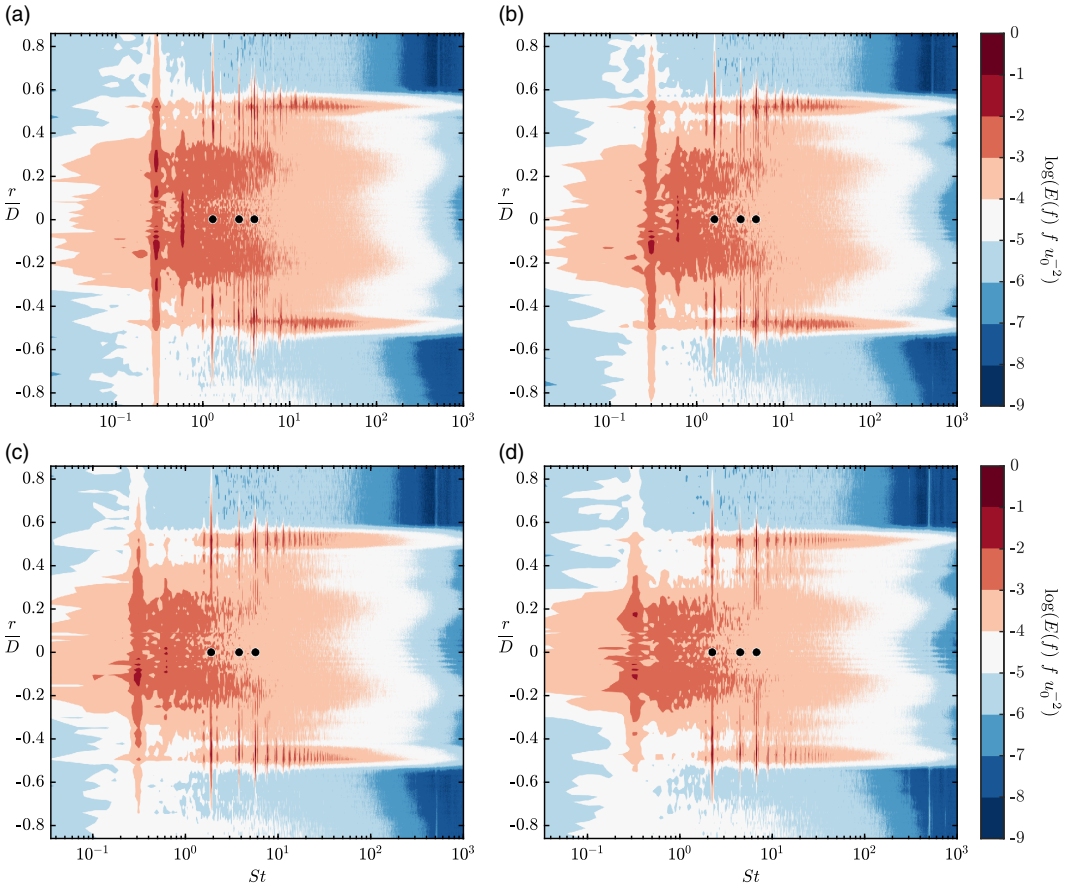

Figure 10. *Premultiplied spectrum displaying spanwise extent of dominant flow features at $x/D = 0.77$ for $\lambda = 4$ (a), 5 (b), 6 (c) and 7 (d). Black dots correspond to St for $f_{rot}, 2f_{rot}, 3f_{rot}$.*

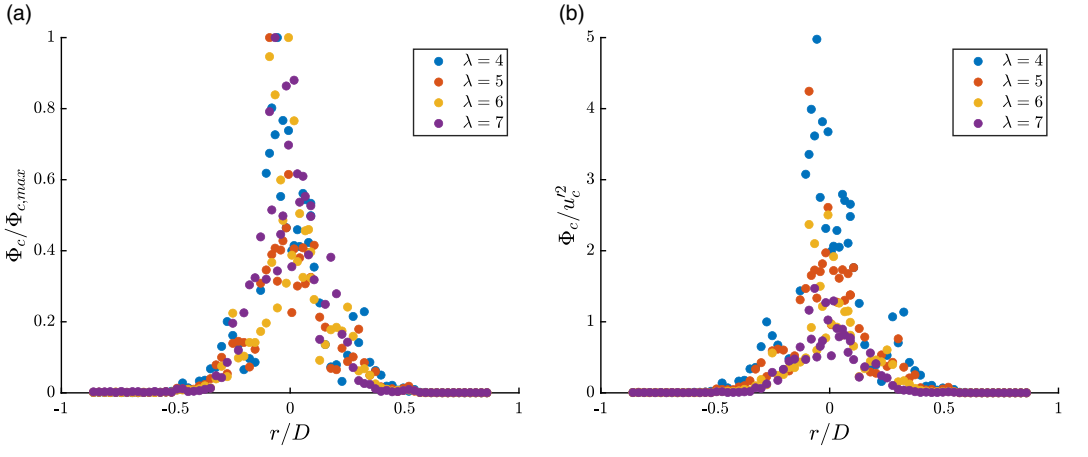

Figure 11. *Peaks of the premultiplied spectrum at $x/D = 0.77$ associated with the maximums in the range of $0.55 < St < 0.65$, Φ_c. In (a), the premultiplied spectrum is non-dimensionalised by the greatest signature magnitude associated with the core shedding, $\Phi_{c,max}$. In (b), the premultiplied spectrum is non-dimensionalised by the variance at the centreline, $u_c'^2$.*

https://doi.org/10.1017/flo.2025.10037 Published online by Cambridge University Press

4. Conclusions

In this study, the wakes of a wind turbine were investigated at $Re_D = 4 \times 10^6$ for a range of tip speed ratios, $4 < \lambda < 7$. The near- and intermediate-wake regions were studied using nanoscale hot-wire anemometry. Across this λ range, C_T was relatively constant, a design feature that is uncommon for most wind turbine geometries. Whereas some past wind turbine studies have been unable to decouple the influence of C_T and λ on turbine wake evolution, the trends observed for this turbine could be more strongly related to the turbine's rotation.

Overall, the analysis of the high Reynolds number wake data showed that the tip speed ratio has a significant effect on the wake dynamics. It was further shown that mean deficit velocity profiles were invariant in the near wake, whereas the profiles in the intermediate wake showed a dependence on λ, with a smaller λ leading to a more rapid wake recovery. This observation contradicted a recent tip speed ratio parametric study conducted at an order of magnitude lower Reynolds number (Bayron et al., 2024), but an investigation of the axial variance profiles indicated stronger turbulence levels for lower tip speed ratios across most of the downstream positions tested, specifically $1.52 < x/D < 5.52$. However, the variance profiles alone were insufficient for deciphering which flow features contribute to the modified turbulence levels.

Within the near wake, the turbulent energy as measured by the variance profiles, was found to decrease with increasing λ in the proximity of the tip vortex, whereas it was close to independent of λ at the wake core for the vast majority of scales. Through spectral analysis, the energy content of the turbulent length scales in the proximity of the tip vortex were investigated to determine which scales contributed to the higher turbulence levels at smaller tip speed ratios. The tip vortex was shown to have a broadband effect across a wide range of scales, which elevates the turbulence levels in its proximity. However, at the farthest downstream point of the near wake ($x/D = 2.02$), the energy content of the tip vortex scales was found to be greater for smaller λ, coinciding with the same trends found in the variance. The trends in the energy content of the tip vortex scales persisted into the intermediate wake, again supporting the same trends found in the variance profiles for the same region. The relationship between the tip vortex-scale energy content and λ supports the hypothesis that a smaller tip speed ratio accelerates wake recovery within the intermediate wake due to a stronger tip vortex and its more energetic turbulence. The wake recovery trend with tip vortex strength indicates the importance of accurately resolving the tip vortex and its broadband effect in future modelling efforts.

Wake meandering and the wake core structure were found to dominate the low-frequency content of the wake. The wake core structure was found to have a spectral peak at $St = 0.6$, independent of λ, contradicting previous findings (Viola et al., 2014; Iungo et al., 2013). The λ invariance is a strong indication that the core structure is not strictly governed by the turbine blades, but is rather due to a bulk geometric feature of the unique turbine. This turbine was based on a Vestas V27 turbine, but the model's chord length was increased by a factor of 3 to prevent blade stall (Miller, 2018). The higher solidity of the tested turbine versus commercially available turbines may explain the λ invariance of the core structure. Future experiments studying solidity effects would assist with understanding how turbine solidity affects the core structure.

The strength of wake meandering and the wake core signature are both found to be dependent on the tip speed ratio; their magnitudes decrease with increasing λ. Furthermore, the wake core structure is shown to have a greater downstream extent with decreasing tip speed ratio. Although the spanwise extent of the wake core structure was found to be invariant with λ, the relative strength of the core structure across the span was found to be dependent; decreasing λ produced a stronger core structure. The stronger wake core structure relative to the turbulence in the core at lower tip speed ratio was determined to be the reason for its increased longevity.

Acknowledgements. The authors would like to acknowledge the support of the National Science Foundation under Grant No. CBET 1652583 (Program Manager R. Joslin).

Data availability statement. Data are available from the corresponding author, A.P., upon reasonable request.

https://doi.org/10.1017/flo.2025.10037 Published online by Cambridge University Press

Author contributions. Alexander Piqué: methodology, data curation, writing-original draft preparation, formal analysis, investigation, visualisation. Mark A. Miller: writing-review and editing, methodology. Marcus Hultmark: writing-review and editing, supervision

Funding statement. This work was supported by the National Science Foundation under Grant No. CBET 1652583.

Competing interests. The authors declare that they have no known competing financial interests or personal relationships that could have appeared to influence the work reported in this paper.

References

Alam, M. M., Zhou, Y., Yang, H. X., Guo, H., & Mi, J. (2010). The ultra-low Reynolds number airfoil wake. *Experiments in Fluids*, *48*(1), 81–103.

Ashton, R., Viola, F., Camarri, S., Gallaire, F., & Iungo, G. V. (2016). Hub vortex instability within wind turbine wakes: Effects of wind turbulence, loading conditions, and blade aerodynamics. *Physical Review Fluids*, *1*(7), 073603.

Bahaj, A. S., Molland, A. F., Chaplin, J. R., & Batten, W. M. J. (2007). Power and thrust measurements of marine current turbines under various hydrodynamic flow conditions in a cavitation tunnel and a towing tank. *Renewable Energy*, *32*(3), 407–426.

Bastankhah, M., & F., Porté-Agel. (2016). Experimental and theoretical study of wind turbine wakes in yawed conditions. *Journal of Fluid Mechanics*, *806*, 506–541.

Bastankhah, M., & Porté-Agel, F. (2015). A wind-tunnel investigation of wind-turbine wakes in yawed conditions. *Journal of Physics: Conference Series*, *625*(1), 012014.

Bayron, P., Kelso, R., & Chin, R. (2024). Experimental investigation of tip-speed-ratio influence on horizontal-axis wind turbine wake dynamics. *Renewable Energy*, *225*, 120201.

Brunner, C. E., Kiefer, J., Hansen, M. O. L., & Hultmark, M. (2021). Study of reynolds number effects on the aerodynamics of a moderately thick airfoil using a high-pressure wind tunnel. *Experiments in Fluids*, *62*(8), 1–17.

Ceccotti, C., Spiga, A., Bartl, J., & Sætran, L. (2016). Effect of upstream turbine tip speed variations on downstream turbine performance. *Energy Procedia*, *94*, 478–486.

Chamorro, L. P., Arndt, R. E. A., & Sotiropoulos, F. (2012). Reynolds number dependence of turbulence statistics in the wake of wind turbines. *Wind Energy*, *15*(5), 733–742.

Chamorro, L. P., Hill, C., Morton, S., Ellis, C., Arndt, R. E. A., & Sotiropoulos, F. (2013). On the interaction between a turbulent open channel flow and an axial-flow turbine. *Journal of Fluid Mechanics*, *716*, 658–670.

Devinant, P., Laverne, T., & Hureau, J. (2002). Experimental study of wind-turbine airfoil aerodynamics in high turbulence. *Journal of Wind Engineering and Industrial Aerodynamics*, *90*, 689–707.

Ebert, P. R., & Wood, D. H. (1999). The near wake of a model horizontal-axis wind turbine—II. General features of the three-dimensional flowfield. *Renewable Energy*, *18*(4), 513–534.

Ebert, P. R., & Wood, D. H. (2001). The near wake of a model horizontal-axis wind turbine: Part 3: Properties of the tip and hub vortices. *Renewable Energy*, *22*(4), 461–472.

Eggleston, D. M., & Stoddard, F. (1987). *Wind turbine engineering design*. Van Nostrand Reinhold Co. Inc.

El Fajri, O., Bowman, J., Bhushan, S., Thompson, D., O'Doherty, T. (2022). Numerical study of the effect of tip-speed ratio on hydrokinetic turbine wake recovery. *Renewable Energy*, *182*, 725–750.

Espana, G., Aubrun, S., Loyer, S., & Devinant, P. (2011). Spatial study of the wake meandering using modelled wind turbines in a wind tunnel. *Wind Energy*, *14*(7), 923–937.

Fan, Y., Arwatz, G., Van Buren, T. W., Hoffman, D. E., & Hultmark, M. (2015). Nanoscale sensing devices for turbulence measurements. *Experiments in Fluids*, *56*(7), 1–13.

Felli, M., Camussi, R., & Di Felice, F. (2011). Mechanisms of evolution of the propeller wake in the transition and far fields. *Journal of Fluid Mechanics*, *682*, 5–53.

Foti, D., Yang, X., Guala, M., & Sotiropoulos, F. (2016). Wake meandering statistics of a model wind turbine: Insights gained by large eddy simulations. *Physical Review Fluids*, *1*(4), 044407.

Gaster, M. (1967). *The structure and behaviour of separation bubbles* (*Tech. Rep.* 3595, Aeronautical Research Council).

Heisel, M., Hong, J., & Guala, M. (2018). The spectral signature of wind turbine wake meandering: A wind tunnel and field-scale study. *Wind Energy*, *21*(9), 715–731.

Howard, K. B., Singh, A., Sotiropoulos, F., & Guala, M. (2015). On the statistics of wind turbine wake meandering: An experimental investigation. *Physics of Fluids*, *27*(7), 075103.

Hu, H., Yang, Z., & Sarkar, P. (2012). Dynamic wind loads and wake characteristics of a wind turbine model in an atmospheric boundary layer wind. *Experiments in Fluids*, *52*(5), 1277–1294.

Iungo, G. V., Viola, F., Camarri, S., Porté-Agel, F., & Gallaire, F. (2013). Linear stability analysis of wind turbine wakes performed on wind tunnel measurements. *Journal of Fluid Mechanics*, *737*, 499–526.

Johansson, P. B. V., & George, W. K. (2006). The far downstream evolution of the high-Reynolds-number axisymmetric wake behind a disk. Part 1. Single-point statistics. *Journal of Fluid Mechanics*, *555*, 363–385.

https://doi.org/10.1017/flo.2025.10037 Published online by Cambridge University Press

Kang, S., Yang, X., & Sotiropoulos, F. (2014). On the onset of wake meandering for an axial flow turbine in a turbulent open channel flow. *Journal of Fluid Mechanics*, *744*, 376–403.

Larsen, G. C., Aagaard Madsen, H., & Bingöl, F. (2007). *Dynamic wake meandering modeling* (Tech. Rep., Risøe National Lab).

Lignarolo, L. E. M., Ragni, D., Krishnaswami, C., Chen, Q., Ferreira, C. J. S., & Van Bussel, G. J. W. (2014). Experimental analysis of the wake of a horizontal-axis wind-turbine model. *Renewable Energy*, *70*, 31–46.

Lignarolo, L. E. M., Ragni, D., Scarano, F., Ferreira, C. J. S., & Van Bussel, G. J. W. (2015). Tip-vortex instability and turbulent mixing in wind-turbine wakes. *Journal of Fluid Mechanics*, *781*, 467–493.

Llorente, E., Gorostidi, A., Jacobs, M., Timmer, W. A., Munduate, X., & Pires, O. (2014). Wind tunnel tests of wind turbine airfoils at high Reynolds numbers. *Journal of Physics: Conference Series*, *524*, 012012.

Medici, D., & Alfredsson, P. H. (2006). Measurements on a wind turbine wake: 3D effects and bluff body vortex shedding. *Wind Energy: An International Journal for Progress and Applications in Wind Power Conversion Technology*, *9*(3), 219–236.

Miller, M. A. M. 2018, High Reynolds number horizontal and vertical axis wind turbine experiments. *PhD thesis*, Princeton University).

Miller, M. A., Kiefer, J., Westergaard, C., Hansen, M. O. L., & Hultmark, M. (2019). Horizontal axis wind turbine testing at high Reynolds numbers. *Physical Review Fluids*, *4*(11), 110504.

Narasimha, R. (1985). The laminar-turbulent transition zone in the boundary layer. *Progress in Aerospace Sciences*, *22*(1), 29–80.

Odemark, Y., & Fransson, J. H. M. (2013). The stability and development of tip and root vortices behind a model wind turbine. *Experiments in Fluids*, *54*(9), 1–16.

Okulov, V. L., Naumov, I. V., Mikkelsen, R. F., Kabardin, I. K., & Sørensen, J. N. (2014). A regular Strouhal number for large-scale instability in the far wake of a rotor. *Journal of Fluid Mechanics*, *747*, 369–380.

Okulov, V. L., & Sørensen, J. N. (2007). Stability of helical tip vortices in a rotor far wake. *Journal of Fluid Mechanics*, *576*, 1–25.

Piqué, A. (2023). High Reynolds number wind tunnel studies of a wind turbine's wake (*PhD thesis*, Princeton University).

Piqué, A., Miller, M. A., & Hultmark, M. (2022a). Dominant flow features in the wake of a wind turbine at high Reynolds numbers. *Journal of Renewable and Sustainable Energy*, *14*, 033304.

Piqué, A., Miller, M. A., & Hultmark, M. (2022b). Laboratory investigation of the near and intermediate wake of a wind turbine at very high Reynolds numbers. *Experiments in Fluids*, *63*,), 106.

Pires, O., Munduate, X., Ceyhan, O., Jacobs, M., & Snel, H. (2016). Analysis of high Reynolds numbers effects on a wind turbine airfoil using 2D wind tunnel test data. *Journal of Physics: Conference Series*, *753*, 022047.

Porté-Agel, F., Bastankhah, M., & Shamsoddin, S. (2020). Wind-turbine and wind-farm flows: A review. *Boundary-Layer Meteorology*, *174*(1), 1–59.

Samie, M., Marusic, I., Hutchins, N., Fu, M. K., Fan, Y., Hultmark, M., & Smits, A. J. (2018). Fully resolved measurements of turbulent boundary layer flows up to. *Journal of Fluid Mechanics*, *851*, 391–415.

Sarlak, H., Nishino, T., Martínez-Tossas, L. A., Meneveau, C., & Sørensen, J. N. (2016). Assessment of blockage effects on the wake characteristics and power of wind turbines. *Renewable Energy*, *93*, 340–352.

Schümann, H., Pierella, F., & Sætran, L. (2013). Experimental investigation of wind turbine wakes in the wind tunnel. *Energy Procedia*, *35*, 285–296.

Sherry, M., Nemes, A., Jacono, L., David, B., Hugh, M., & Sheridan, J. (2013a). The interaction of helical tip and root vortices in a wind turbine wake. *Physics of Fluids*, *25*(11), 117102.

Sherry, M., Sheridan, J., & Jacono, D. L. (2013b). Characterisation of a horizontal axis wind turbine's tip and root vortices. *Experiments in Fluids*, *54*(3), 1–19.

Sørensen, J. N., Mikkelsen, R. F., Henningson, D. S., Ivanell, S., Sarmast, S., & Andersen, S. J. (2015). Simulation of wind turbine wakes using the actuator line technique. *Philosophical Transactions of the Royal Society A: Mathematical, Physical and Engineering Sciences*, *373*(2035), 20140071.

Tani, I. (1969). Boundary-layer transition. *Annual Review of Fluid Mechanics*, *1*(1), 169–196.

Tedds, S. C., Owen, I., & Poole, R. J. (2014). Near-wake characteristics of a model horizontal axis tidal stream turbine. *Renewable Energy*, *63*, 222–235.

Townsend, A. A. (1956). *The structure of turbulent shear flow*. Cambridge University Press.

Troldborg, N., Sorensen, J. N., & Mikkelsen, R. (2010). Numerical simulations of wake characteristics of a wind turbine in uniform inflow. *Wind Energy: An International Journal for Progress and Applications in Wind Power Conversion Technology*, *13*(1), 86–99.

Vallikivi, M., & Smits, A. J. (2014). Fabrication and characterization of a novel nanoscale thermal anemometry probe. *Journal of Microelectromechanical Systems*, *23*(4), 899–907.

Vinnes, M. K., Gambuzza, S., Ganapathisubramani, B., & Hearst, R. J. (2022). The far wake of porous disks and a model wind turbine: Similarities and differences assessed by hot-wire anemometry. *Journal of Renewable and Sustainable Energy*, *14*(2), 023304.

Viola, F., Iungo, G. V., Camarri, S., Porté-Agel, F., & Gallaire, F. (2014). Prediction of the hub vortex instability in a wind turbine wake: Stability analysis with eddy-viscosity models calibrated on wind tunnel data. *Journal of Fluid Mechanics*, *750*.

Whale, J., Anderson, C. G., Bareiss, R., & Wagner, S. (2000). An experimental and numerical study of the vortex structure in the wake of a wind turbine. *Journal of Wind Engineering and Industrial Aerodynamics*, *84*(1), 1–21.

Widnall, S. E. (1972). The stability of a helical vortex filament. *Journal of Fluid Mechanics*, *54*(4), 641–663.

https://doi.org/10.1017/flo.2025.10037 Published online by Cambridge University Press

Wood, D. H. (1992). On wake modelling at high tip speed ratios. *Wind Engineering*, 291–303.
Yang, X., & Sotiropoulos, F. (2019a). A review on the meandering of wind turbine wakes. *Energies*, *12*(24), 4725.
Yang, X., & Sotiropoulos, F. (2019b). Wake characteristics of a utility-scale wind turbine under coherent inflow structures and different operating conditions. *Physical Review Fluids*, *4*(2), 024604.

Cite this article: Piqué A., Miller M. A. and Hultmark M. (2025). Understanding the effects of rotation on the wake of a wind turbine at high Reynolds number. *Flow*, *5*, E44. https://doi.org/10.1017/flo.2025.10037